

Fast Sweeping Probe System for Characterization of Spokes in ExB Discharges

V. Skoutnev,^{1, a)} P. Dourbal,¹ E. Rodriguez,¹ and Y. Raitsev^{1, b)}

Princeton Plasma Physics Laboratory, Princeton University, Princeton, New Jersey 08543, USA

(Dated: 14 May 2019)

We have developed a rapidly swept, back-to-back 100kHz Langmuir probe system using a tunable compensating network to study the temporal evolution of low frequency oscillations in Penning discharges, Hall Thrusters and other ExB discharges. Experimental validation of the probe system is done at low and high sweeping frequencies in a stable Penning discharge. Then application of the probe system to measurements of plasma parameter fluctuations in a low frequency (4kHz) rotating spoke and an analysis method using the Hilbert transform are shown.

I. INTRODUCTION

Turbulent fluctuations and transient phenomenon are ubiquitous in all laboratory plasmas. A growing need to understand the properties and structure of these phenomena has spurred interest in and development of time resolved Langmuir probe measurements due to their relative simplicity and good spatial resolution. Langmuir probes measure the plasma potential and electron energy distribution function (EEDF) simultaneously based on analysis of the current obtained from sweeping the probe bias voltage. Weighted integration of the EEDF then provides the plasma density and temperature on the time scale at which the probe is swept¹. The temporal and/or spatial variation of these measurements can then be used to study plasma dynamics such as fluctuation-induced particle and heat transport in fusion devices²⁻⁴, and coherent oscillatory modes in, for example, Hall thrusters and linear plasma devices⁵⁻⁸.

For low sweeping frequencies (around 1kHz or below), Langmuir probes are typically constructed by connecting a driving voltage source through a small resistor to a metallic end immersed in the plasma. At a given bias voltage, the current collected from the plasma flows through the resistor and can be directly measured. However, at higher sweeping frequencies f of the driving voltage, with peak to peak voltage range V_{pp} , the reactive current $I_R = C \frac{dV}{dt} = \pi f C V_{pp}$ arising from the capacitance C of the coaxial cables ($\sim 100\text{pF/m}$) and circuitry begins to dominate the true plasma current I_p for $f \gtrsim I_p / (\pi C V_{pp})$, and must somehow be compensated. This is especially relevant for larger plasma devices such as tokamaks, Hall thruster chambers, and linear plasma devices where cables may need to be several meters long. For example in a typical low temperature plasma measurement at very negative bias voltages where the current is smallest, if the ion saturation current is $I_p \approx I_{sat} \approx 0.5\text{mA}$ and a probe system has a

net capacitance of 1nF from $\sim 10\text{m}$ of cables with a $V_{pp} = 50\text{V}$ sweeping voltage range, the reactive current becomes comparable to I_p at around $f = 3\text{kHz}$.

Many solutions to compensate the reactive current have been implemented with varying degrees of success. One idea is to use an additional null probe that runs along the Langmuir probe but is insulated from the plasma, so that both have the same capacitance^{3,9-11}. The currents through the probes can be separately measured and then subtracted during post-processing to obtain the true plasma current. This approach allows for nearly exact capacitance cancellation between the probes and has been successfully shown to be able to sweep up to 400kHz in the High-speed dual Langmuir probe system¹².

Another method consists of using variable capacitors in the internal circuitry of the probe system to simulate and compensate the stray capacitances^{2,4}. This method requires calibration at each sweeping frequency, but does not require construction of a parallel null probe: the probe system is directly connected to a standard Langmuir probe.

In this article, we describe the design and application of a variable capacitor compensation scheme that allows fast sweep ($f \gtrsim 3\text{kHz}$ where $I_R \gtrsim I_{sat}$) measurements. In contrast to previous designs, we measure differential current at low voltages through a particular setup of insulated power amplifiers, avoiding issues with measurements at high sweeping voltages. Section II describes the principle and schematic behind the fast sweep probe system. Section III describes validation of the probe system inside a stable Penning discharge by benchmarking against an accepted commercial probe system, the Multifunctional Plasma Probe Analyzer¹³. Section IV describes an application of the fast sweep system to a 4kHz rotating spoke and an analysis method of the measured fluctuations that implements the Hilbert transform. We find that particle transport due to azimuthal electric field fluctuations across an axial magnetic field contribute approximately 33% of the anomalous transport in a Penning discharge undergoing spoke oscillations.

^{a)}Electronic mail: vskoutne@pppl.gov

^{b)}Electronic mail: yraitses@pppl.gov

II. PROBE SYSTEM ELECTRONICS

The general technique for compensating reactive currents arising from fast sweeping is based on 1) creating a compensating channel with reactive impedance equivalent to the real probe / chamber system, and 2) finding the difference between the current across the created channel and the probe channel to obtain the real plasma current.

A significant difficulty with this approach is the need to resolve the small plasma current (mA) that is the difference between two signals each riding high voltages ($\pm 50/100\text{V}$) at high frequencies (1-100kHz). The current measurements at each channel are typically done across sensing shunts using isolation amplifiers and current meters capable of providing a high dynamic range at the high sweeping frequencies¹². Amplifiers and current meters satisfying all of the specifications are often either expensive, not commercially available, or prohibitively difficult to construct.

We have implemented a method of creating a compensating channel and measuring differential current free of the above difficulty. By using two (A and B in Figure 1) fully insulated power amplifiers (including their power supplies), driven with opposite polarities by a common voltage source (C in Figure 1), we are able to connect their low voltage outputs together at a reference point (D in Figure 1) grounded to the chamber through a single sensing shunt. For a compensating capacitor calibrated to match the capacitance of the probe channel, the reactive currents in the two channels are identical and the result of analog subtraction (due to the polarity flip of the power amplifiers) at point D leaves only the small plasma current to be measured across the shunt with a single input, low noise amplifier (a demonstration is shown in the Appendix). Since this low noise amplifier is not exposed to the high sweeping voltages, it can have milder specifications and the current meter can have a lower dynamic range to obtain the same sensitivity as a higher dynamic range current meter measuring at high voltages.

Measurement is done by connecting the low noise amplifier to a PicoScope 5000 series oscilloscope (DAQ in Figure 1) capable of a sampling rate of 125MS/s with 14 bit resolution. We use an asymmetric sawtooth waveform for the biasing voltage to provide a uniform distance between samples on the I-V trace and analyze in the region where $\frac{dV}{dt} > 0$, which corresponds to approximately 1000 samples for each single I-V trace at 100kHz sweeping.

This design allows us to perform measurements of Langmuir I-V traces and their derivatives up to sweeping frequencies of 100kHz. Calibrating at a given sweeping frequency consists of substituting the Langmuir probe in Figure 1 with a resistor and adjusting the variable compensating capacitor within its range of $\lesssim 1400\text{pF}$ until there is no phase lag between applied AC voltage and measured current. The calibration does not account for the additional impedance of the Langmuir probe. The extra capacitance from a Langmuir probe of area A and

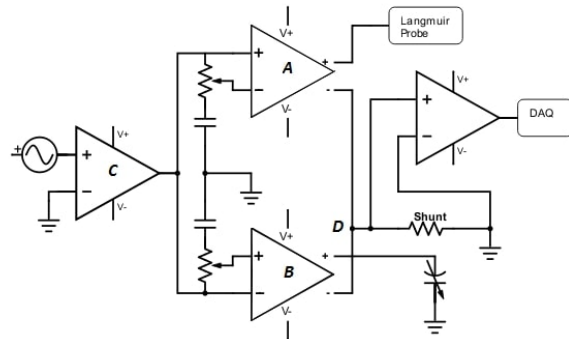


FIG. 1. Electronic schematic of the main components of the fast sweep probe system. Point D is where reactive currents undergo analog subtraction due to their inverted input voltage signals and the remaining plasma current is measured across the shunt using a low noise amplifier in parallel.

a typical probe sheath on the order of a Debye length, λ_D , is on the order of $0.5\epsilon_0 A/\lambda_D \approx 1\text{pF}$, where ϵ_0 is the vacuum permittivity. This $\sim 1\text{pF}$ sheath capacitance is, however, negligible compared to the original $\sim 1\text{nF}$ capacitance of the cables and circuitry.

III. PROBE SYSTEM VALIDATION

To validate the accuracy of our probe system across the range of sweeping frequencies 1-100kHz, we compare experimental measurements in a stable Penning discharge against the Multifunctional Plasma Probe Analyzer (MFPA) developed by Plasma Sensors, a tested and accepted commercial probe system that provides high energy resolution and dynamic range EEDF measurements¹³. The MFPA uses a reference probe to eliminate distortions associated with floating potential fluctuations and typically averages ≥ 100 sweeps at 1kHz to produce robust I-V traces.

We setup a stable (no large plasma oscillations present) Argon Penning discharge at 1.5mTorr with a crossed radial electric and 30G axial magnetic field, corresponding to an electron gyroradius of $\rho_g \approx 1\text{mm}$. A cylindrical, tungsten Langmuir probe (diameter $d_p = 0.1\text{mm}$ and length 3mm) is placed perpendicular to the magnetic field where beam effects are not present and an isotropic, near-Maxwellian electron population is present¹⁴. A few gyroradii outside ($10\rho_g \approx 1\text{cm}$) the axis-centered beam, isotropy is maintained primarily by electron-neutral collisions with a mean free path of 50cm and collision frequency of 0.5MHz, much faster than the 4kHz spoke oscillations. The Langmuir probe is biased relative to the metal walls of the chamber, which have large enough area to compensate for the current flowing into the probe. Note that, although electrons are magnetized, we may

still apply conventional probe theory for non-magnetized plasmas because the ratio of the probe radius to the gyroradius $\frac{d_p}{2\rho_g} \approx 0.05$ is small^{15,16}.

For the validation experiment, at each sweeping frequency of the fast sweep probe system (FSPS), 10 sets of 50 back-to-back I-V traces are taken followed by the recording of an identical number of traces at 1kHz using MFPA on the same Langmuir probe. Alternating between probe systems accounts for any drifts in the discharge on the timescale of minutes over the course of the experiment (recalibration of FSPS for each frequency takes a few minutes).

To compute the plasma potential and the EEDF from the data sets we implement the Druyvesteyn method for isotropic energy distributions^{16,17}. The EEDF has been shown to be the most reliable probe diagnostic for low temperature laboratory and processing plasmas¹⁸. The Druyvesteyn method starts with taking the second derivative of the plasma current $I(V)$ with respect to the bias voltage and finding the plasma potential V_p from where $I''(V) = 0$. The EEDF $F(\varepsilon)$ and the related electron energy probability function (EEDF) $f_p(\varepsilon) = F(\varepsilon)/\sqrt{\varepsilon}$ is then given by the Druyvesteyn formula¹⁶:

$$\frac{d^2 I}{d^2 V} = -\frac{e^2 S_p}{4} \sqrt{\frac{2e}{mV}} F(eV) = \frac{e^3 S_p}{2\sqrt{2m}} f_p(eV) \quad (1)$$

where S_p is the probe area, e is the electron charge, m is the electron mass, and $V \leq 0$ is taken to be relative to V_p . The plasma density and effective temperature are then found by integration of the EEDF¹⁶.

$$N = \frac{2\sqrt{2m}}{|e|S_p} \int_0^{-\infty} I''(V) \sqrt{|V|} dV \quad (2)$$

$$T_e = \frac{4\sqrt{2m}/|e|}{3NS_p} \int_0^{-\infty} I''(V) |V|^{3/2} dV \quad (3)$$

For $f_{\text{sweep}} \lesssim f_{\text{pi}} \approx 10^6 \text{ Hz}$ (the ion plasma frequency), collisionless, thin sheath theory holds and polarization and sheath capacitance effects are negligible¹⁹. 100kHz is safely within this limit, so any variations in the measured plasma parameters with increasing sweeping frequency are an effect of the probe system electronics, analysis technique, errors in calibration, and drifts in the discharge between measurements.

We find that measured plasma parameters (Figure 2) with the two probe systems have relative differences of around 10% to 20%, whose origin can be seen in the comparison of four representative EEDFs in Figure 3. Note that the peaks of all the EEDFs occur between 1.5 and 2eV, which is less than half the average measured temperature $T_e \approx 4\text{eV}$ of the discharge and therefore satisfies the criterion for acceptable EEDF measurements given by V.A. Godyak (2011)¹⁶. In the lower energy range $\lesssim 2T_e$, where the majority of the electron population resides, the $f_{\text{p,FSPS}}^{100\text{kHz}}$ is larger while $f_{\text{p,FSPS}}^{1\text{kHz}}$ is smaller than $f_{\text{p,MFPA}}^{1\text{kHz}}$.

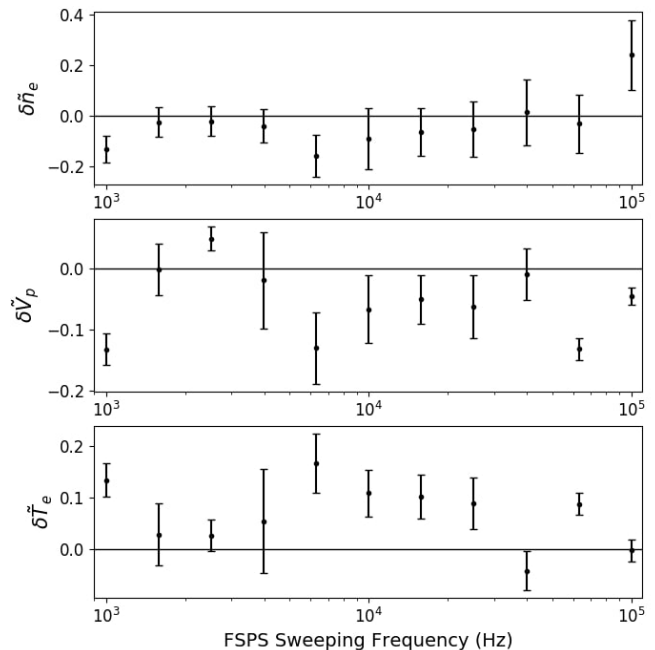


FIG. 2. Relative error (e.g. $\delta \tilde{n}_e = \frac{\delta n_e}{n_e}$) between FSPS and MFPA are shown versus sweeping frequency of FSPS: δ in density (top), plasma potential (middle), and temperature (bottom). MFPA control measurements are always taken at 1kHz. The mean and standard deviation (error bars) are computed from 10 sets of 50 measured plasma parameters at each FSPS sweeping frequency.

This corresponds to the relatively higher and lower measured density, respectively, seen in Figure 2. The difference in temperature measurements occurs due to different slopes of the EEDFs ($\log(f_p(\varepsilon)) \propto -1/T_e$). From the top and bottom panel of Figure 3, it is roughly visible that $f_{\text{p,FSPS}}^{1\text{kHz}}$ has a smaller average slope while $f_{\text{p,FSPS}}^{100\text{kHz}}$ has similar average slope compared to the slope of $f_{\text{p,MFPA}}^{1\text{kHz}}$, corresponding to the relatively higher and similar measured effective temperature, respectively, seen in Figure 2. $f_{\text{p,FSPS}}^{39\text{kHz}}$ is quantitatively similar to $f_{\text{p,FSPS}}^{1\text{kHz}}$.

At higher energies $\varepsilon \gtrsim 3T_e$ the coefficient of variation rises above $\frac{\sigma}{\mu} = 0.5$ at $4.4T_e$, $4.7T_e$, and $3.7T_e$ for $f_{\text{p,FSPS}}^{1\text{kHz}}$, $f_{\text{p,FSPS}}^{39\text{kHz}}$, and $f_{\text{p,FSPS}}^{100\text{kHz}}$, respectively, where $\mu(\varepsilon)$ and $\sigma(\varepsilon)$ are the mean and standard deviation of the energy bins. We choose $\frac{\sigma}{\mu} = 0.5$ as the cutoff above which probe system distortions and electronic noise become too significant for analysis and therefore we restrict EEDF analysis to energy ranges $\varepsilon_{\text{max}} \lesssim 3.7T_e \approx 13\text{eV}$ in future measurements at higher sweeping frequencies. Analysis of other sweeping frequencies shows that ε_{max} is roughly unchanged below 39kHz and begins to decrease for higher frequencies.

The coefficient of variation ($\frac{\sigma}{\mu}$) of MFPA is lower than that of FSPS over the whole energy range because MFPA has lower internal electronic noise than FSPS due to the

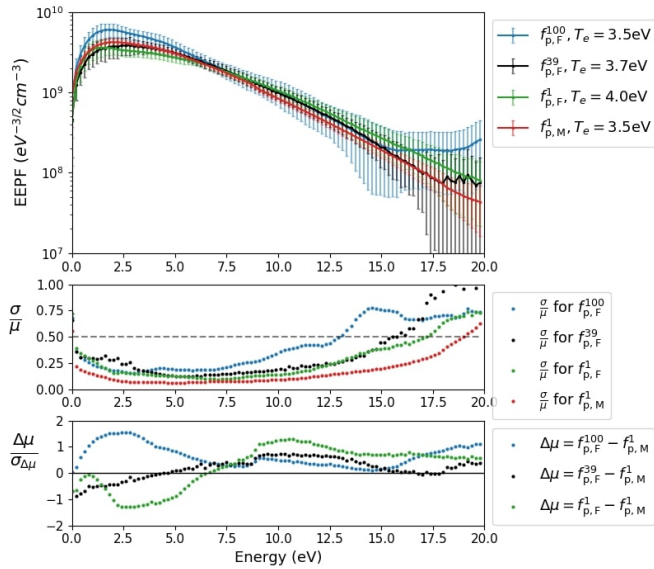


FIG. 3. Top: Average EEPFs computed by binning the EEPFs from one set of 50 I-V traces for three representative FSPS sweeping frequencies (1kHz, 39kHz, and 100kHz corresponding to $f_{p,F}^1$, $f_{p,F}^{39}$, and $f_{p,F}^{100}$, respectively) and the MFPA at 1kHz ($f_{p,M}^1$) taken during the 10kHz experiment (see Appendix for I-V traces). Error bars are the standard deviation of the energy bins containing values from the 50 individual EEPF's. Middle: The coefficient of variation for each of the EEPFs where $\mu(\varepsilon)$ and $\sigma(\varepsilon)$ are the mean and standard deviation of the energy bins. Bottom: The reciprocal coefficient of variation of the difference between FSPS and MFPA EEPFs.

roughly 100 times higher frequency bandwidth of FSPS's measurement instruments. Sweeping across a resistor we find that MFPA has an internal electronic noise floor of around $7\mu\text{A}$ while the FSPS's is around $200\mu\text{A}$, independent of sweeping frequency. The higher noise floor interferes with resolution of the ion saturation regime and therefore the high energy tail of the EEPF. Density and effective temperature integrals are fortunately primarily determined by the much larger lower energy electron population, limiting the effects of a higher noise floor. This allows FSPS measurements to maintain a relative error within 20% of the low frequency 1kHz MFPA measurements while sweeping across two orders of magnitude higher frequencies.

Overall, sweeping the FSPS at higher frequency leads to both over and under estimation of plasma parameters and to a decrease in the highest resolved energy. Relative differences within 20% between FSPS and MFPA measurements in a quiescent plasma give us confidence to extend the probe system to study plasma parameter variations a non-stationary plasma.

IV. MEASUREMENTS IN A ROTATING SPOKE

The Penning discharge also has a non-stationary state where a robust azimuthally rotating spoke with mode number $m=1$ is present, analogous to the higher mode number spokes found in Hall thrusters^{14,20-22}. Spokes have been linked to anomalous transport in Hall thrusters and known to reduce thruster efficiency^{21,22}. Penning discharges and Hall Thrusters often require an effective electron collision frequency $10^2 - 10^3$ times larger than the classical electron-atom collision frequency to match measurements of the cross field transport, necessitating the presence of other physical mechanisms to explain the enhanced transport²²⁻²⁵. Characterizing the correlations between the fluctuating plasma parameters can help determine the driving factors behind the anomalous transport.

We setup a Xenon Penning discharge at 0.1mTorr with a 40G magnetic field, experimental conditions for which the spoke is present and has a rotation frequency of approximately 4kHz. The Langmuir probe is placed at a fixed location and swept with the FSPS at 50kHz (sufficiently above the Nyquist frequency of the spoke), obtaining a time series of plasma parameter measurements as shown in Figure 4.

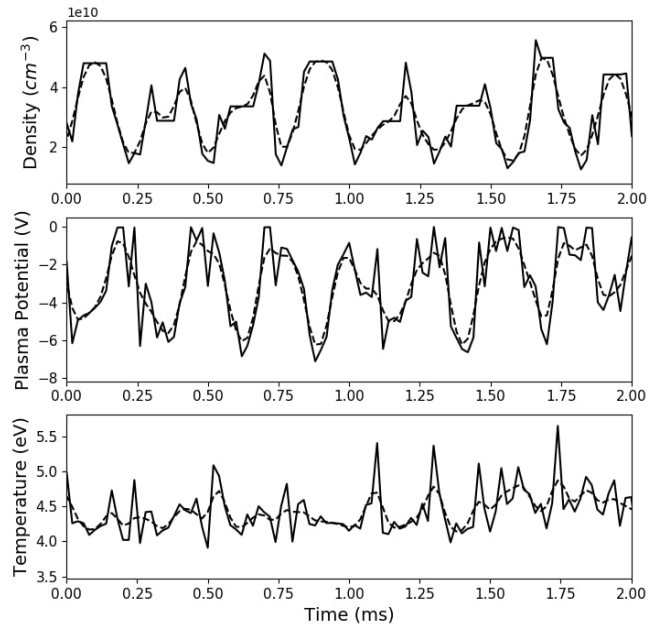


FIG. 4. A sample 2ms time series of FSPS measurements. Each point is one voltage sweep. The underlying dashed curve is the result of a 2nd order low-pass Bessel filter at a cut-off frequency of 10kHz.

Due to the turbulent nature of the spoke, we attempt to statistically capture the azimuthal distribution of the plasma parameters. The general approach is to extract

the instantaneous phase of each plasma parameter relative to the spoke oscillation (defined by the density oscillation in this paper) from the Hilbert transform of its time series and then construct the azimuthal profile by binning over many spoke periods. Hilbert transforms have been applied in experimental plasma data previously, both for fusion devices^{27–29} and Hall thrusters^{30,31}. Temporal variation of the amplitude and frequency of a spoke mode makes nonstationary signal analysis more effective than standard Fourier techniques because it can track instantaneous variation of the amplitude and phase of a given mode³². The Hilbert transform requires a signal with one dominant oscillatory mode, which makes its application to studying breathing and spoke modes in ExB discharges particularly amenable.

The Hilbert transform $\tilde{D}(t)$ of the density time series $D(t)$ results in an analytic signal of the form

$$S_D(t) = D(t) + i\tilde{D}(t) = A_D(t)e^{i\theta_D(t)} \quad (4)$$

where $A_D(t)$ is a slow varying envelope and $\theta_D(t)$ is the fast varying instantaneous phase with $\partial_t\theta_D \approx 4\text{kHz}$ for our spoke. We choose the instantaneous phase $\theta_D(t) = \text{arg}(S_D(t))$ of the density as the reference phase of the spoke oscillation (i.e. the peak in density corresponds to $\theta = 0$). Statistics of the phases of the plasma potential and temperature relative to the spoke density can then be studied either by taking temporal averages of $\theta_P(t) - \theta_D(t)$ and $\theta_T(t) - \theta_D(t)$, respectively, or by analyzing the final phase plots. An example of the resulting phase plot after binning ~ 40 spoke periods (10ms) is shown in Figure 5 and a few representative phase binned EEPFs are plotted in Figure 6 for reference. Compared to the EEPFs in a stationary discharge (Figure 3), the turbulent variation in the spoke itself between periods and increased plasma noise during individual I-V trace measurements leads to a larger variation of EEPF's at a given phase (larger error bars) and smoother EEPFs (due to the need for stronger filtering), respectively.

It is important to note that bandpass filtering the data may be necessary prior to applying the Hilbert transform and binning. A low pass filter allows the Hilbert transform to pick out the low frequency spoke oscillation of interest from any high frequency oscillations or noise. A high pass filter removes slow variations in the mean value of the time series which would uniformly increase the error bars in the phase plot. The bandpass window should be chosen around the primary frequency and increased until either of the two effects begin to distort the phase plot. The phase plot in Figure 5 uses two second order Bessel filters, one with a low pass cut-off frequency of 10kHz and the other with a high pass cut-off frequency of 1kHz.

An estimate of anomalous transport due to radial $E \times B$ transport can be made directly from the phase plot. Variation of the plasma potential azimuthally results in an $E_\phi = \frac{1}{R} \frac{dV}{d\phi}$ which causes radial $v_{E \times B} = \vec{E} \times \vec{B} / B^2$ transport due to the axial magnetic field. Under the

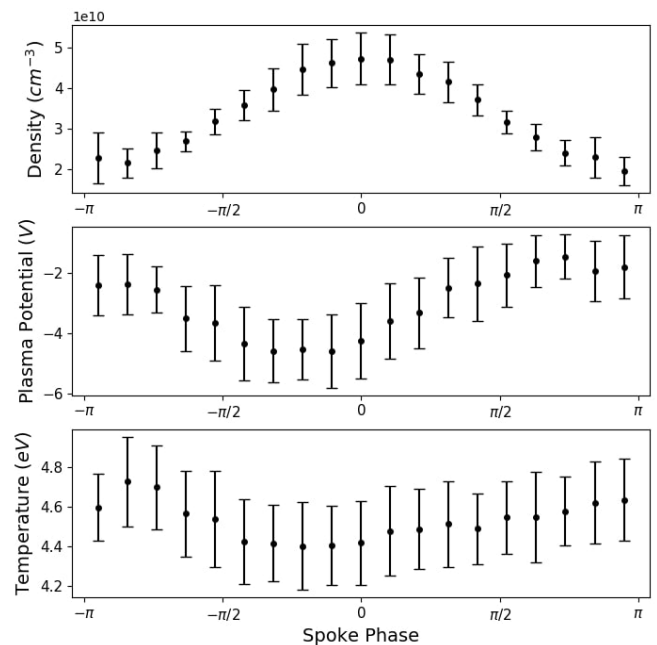


FIG. 5. Azimuthal profiles of plasma parameters inside the spoke determined from binning the filtered plasma parameter time series according to the instantaneous phase of the Hilbert Transform of the density time series. Error bars are the standard deviations of the bins.

assumption that the spoke is rigidly rotating over the timescale of its period, the probe time series measurement is translated to azimuthal variation by $\phi = \theta_D(t)$. With the Langmuir probe at a distance $R = 4\text{cm}$ in our cylindrical Penning discharge of length $L = 38\text{cm}$, we approximate the azimuthal variation to be sinusoidal ($\delta n(t) = \delta n \cos(\theta_D(t))$, $\delta V(t) = \delta V \cos(\theta_D(t) + \theta_{\delta n, \delta V})$) to estimate the total anomalous radial current:

$$I_a = \langle env_{E \times B} \rangle 2\pi RL = -\frac{e\pi L}{B} \delta n \delta V \sin(\theta_{\delta n, \delta V}) \quad (5)$$

Eq. (5) gives $I_a = 0.4\text{A}$ when taking values $\delta n \approx 1.1 \times 10^{10} \text{cm}^{-3}$, $\delta V \approx 1.1\text{V}$, and $\theta_{\delta n, \delta V} \approx -\frac{\pi}{4}$ from the phase plot. This anomalous current is 33% of the total measured discharge current of 1.2A, revealing the potentially important role the spoke plays in cross field transport. Previous experiments in Hall Thrusters have found spoke contribution from 50%³³ or more²³, largely consistent with our result. Further study of radial variation and a separate independent measurement of the phase $\theta_{\delta n, \delta V}$ is necessary to constraint the contribution of the spoke to anomalous transport in the oscillatory mode of the Penning discharge. Such experimental and related simulation studies are underway.

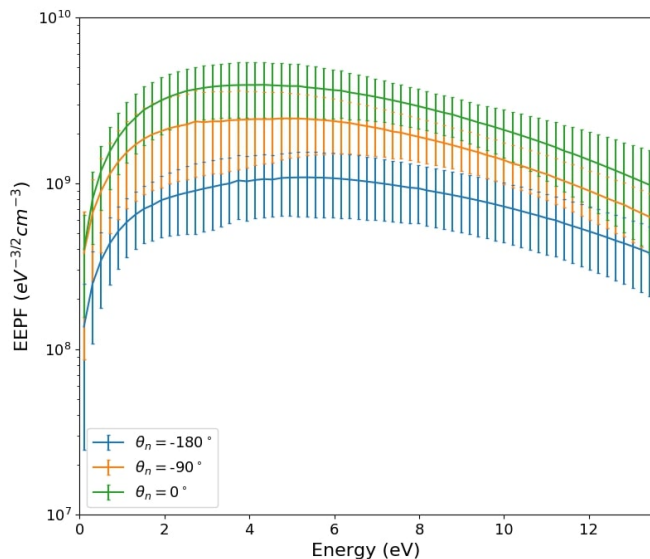


FIG. 6. Representative EEPF's at different phases of the spoke density oscillation. EEPFs are restricted below $3T_e \approx 13.5\text{eV}$.

V. CONCLUSION

We have demonstrated the implementation of a fast sweeping Langmuir probe system that uses fully insulated power amplifiers (including their power supplies) to allow for analog subtraction of reactive and probe currents and thus direct measurement of the plasma current at low voltages. The probe system was shown to provide EEDF, density, plasma potential, and temperature measurements at sweeping frequencies up to 100kHz to within 20% of measurements with MFPA, a well accepted probe system in the field capable of obtaining robust I-V traces at low sweeping frequencies of 1kHz and below^{13,16}.

In an application of the probe system, an analysis procedure of time series data of a 4kHz oscillatory mode in a Penning discharge using the Hilbert transform was presented. The generated phase plot using the Hilbert transform approach gives a clear picture of the average magnitude of fluctuations of the plasma parameters and their mutual phase differences for a dominant mode in an $E \times B$ discharge. This allowed for an estimation of particle transport due to azimuthal electric field fluctuations which showed that a rotating spoke contributes approximately 33% of the anomalous transport in a Penning discharge undergoing spoke oscillations.

VI. ACKNOWLEDGMENTS

The authors are indebted to Alex Merzhevskiy for engineering support on probe systems and the Penning

device. We are grateful to Igor Kaganovich, Ivan Romanov, and Andrei Smolyakov for discussions on spoke phenomenon. Thanks also to Valery Godyak and Benjamin Alexandrovich for support on operation of MFPA.

This work was supported by the Air Force Office of Scientific Research (AFOSR).

VII. APPENDIX

To demonstrate the principle behind the compensation network, we show the result of measurement using FSPS of the current from a $R = 3.3\text{k}\Omega$ resistor driven at 50kHz with a 10V amplitude sine wave offset by +10V. The top panel of Figure 7 shows opposite polarity of the driving voltage going into amplifiers A and B of Figure 1. The bottom panel shows the measured I-V curve for the resistor when the compensating capacitor is either to 0 (no compensation) or is calibrated (with compensation). As expected, compensating the capacitance of the cables leads to the I-V trace of a resistor with $I = V/R$.

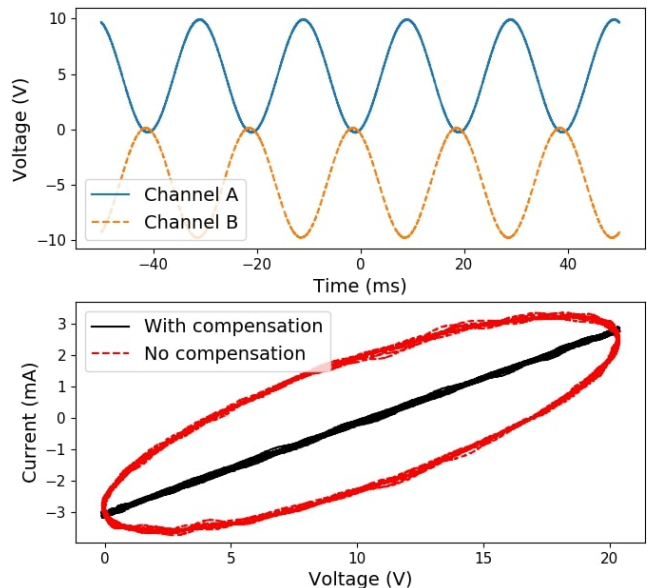


FIG. 7. Top: Shown are the voltage inputs into amplifiers A and B in Figure 3 when the driving signal at C is a 10V amplitude sine wave with a +10V offset. Bottom: The I-V curve for a 3.3kOhm resistor in place of the Langmuir probe with and without a compensating capacitor.

We include I-V traces corresponding to the EEPFs in the validation experiment (Section 3) for reference. Each I-V trace in Figure 8 is the average of one set of 50 traces. Variation in the electron saturation current region near the plasma potential is normal in a discharge. However, at lower bias voltages, FSPS struggles to resolve the small ion current due to its larger internal noise, leading to the deviations of the MFPA and FSPS EEPFs at higher

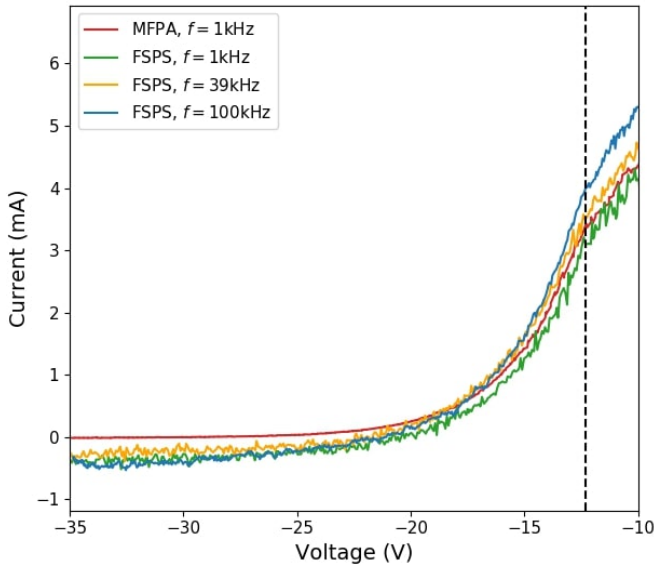


FIG. 8. I-V traces corresponding to the EEPFs in Figure 3 during the validation experiment for different probe systems and sweeping frequencies. Dashed vertical line is located at the plasma potential.

energies in Figure 3 ($\gtrsim 13\text{eV}$ on the EEPFs corresponds to $\lesssim -25\text{V}$ on the I-V traces).

- ¹J.D. Swift and M.J.R. Schwar, *Electrical Probes for Plasma Diagnostics* (Ilfie Books, London, 1970).
- ²M. Schubert, M. Endler, and H. Thomsen, *Review of Scientific Instruments* 78, 053505 (2007).
- ³L. Giannone, R. Balbn, H. Niedermeyer, M. Endler, G. Herre, C. Hidalgo, A. Rudyj, G. Theimer, and P. Verplanke, *Physics of Plasmas* 1, 3614 (1994).
- ⁴P.C. Liewer, J.M. Mcchesney, S.J. Zweben, and R.W. Gould, *Physics of Fluids* 29, 309 (1986).
- ⁵E. Chesta, C. Lam, N. Meezan, D. Schmidt, and M. Cappelli, *IEEE Transactions on Plasma Science* 29, 582 (2001).
- ⁶M. Sekerak, M. Mcdonald, R. Hofer, and A. Gallimore, 2013 IEEE Aerospace Conference (2013).
- ⁷E. Wallace, E. Thomas, A. Eadon, and J.D. Jackson, *Review of Scientific Instruments* 75, 5160 (2004).
- ⁸W. Gekelman, H. Pfister, Z. Lucky, J. Bamber, D. Leneman, and J. Maggs, *Review of Scientific Instruments* 62, 2875 (1991).

- ⁹G. Chiodini, C. Riccardi, and M. Fontanesi, *Review of Scientific Instruments* 70, 2681 (1999).
- ¹⁰F.F. Chen, *Plasma Diagnostic Techniques*, edited by R. H. Huddleston (Academic, New York, 1965).
- ¹¹T.F. Yang, Q.X. Zu, and P. Liu, *Review of Scientific Instruments* 66, 3879 (1995).
- ¹²R.B. Lobbia and A.D. Gallimore, *Review of Scientific Instruments* 81, 073503 (2010).
- ¹³MFPA Probe System <http://www.plasmasensors.com/>
- ¹⁴Y. Raitses, I. Kaganovich, A. Smolyakov, 2015 International Electric Propulsion Conference (2015).
- ¹⁵Y.M. Kagan and V.I. Perel, *Soviet Physics Uspekhi* 6, 767 (1964).
- ¹⁶V.A. Godyak and V.I. Demidov, *Journal of Physics D: Applied Physics* 44, 233001 (2011).
- ¹⁷M.J. Druyvesteyn and F.M. Penning, *Reviews of Modern Physics* 12, 87 (1940).
- ¹⁸V.A. Godyak and B.M. Alexandrovich, *Journal of Applied Physics* 118, 233302 (2015).
- ¹⁹R.B. Lobbia and A.D. Gallimore, *Physics of Plasmas* 17, 073502 (2010).
- ²⁰Y. Sakawa, C. Joshi, P.K. Kaw, F.F. Chen, and V.K. Jain, *Physics of Fluids B: Plasma Physics* 5, 1681 (1993).
- ²¹J.A. Carlsson, I.D. Kaganovich, A.V. Khrabrov, A. Smolyakov, D. Sydorenko, and Y. Raitses, 2015 IEEE International Conference on Plasma Sciences (ICOPS) (2015).
- ²²J. Carlsson, I. Kaganovich, A. Powis, Y. Raitses, I. Romadanov, and A. Smolyakov, *Physics of Plasmas* 25, 061201 (2018).
- ²³C.L. Ellison, Y. Raitses, and N.J. Fisch, *Physics of Plasmas* 19, 013503 (2012).
- ²⁴C. Boniface, L. Garrigues, G.J.M. Hagelaar, J.P. Boeuf, D. Gawron, and S. Mazouffre, *Applied Physics Letters* 89, 161503 (2006).
- ²⁵J.B. Parker, Y. Raitses, and N.J. Fisch, *Applied Physics Letters* 97, 091501 (2010).
- ²⁶A.T. Powis, J.A. Carlsson, I.D. Kaganovich, Y. Raitses, and A. Smolyakov, *Physics of Plasmas* 25, 072110 (2018).
- ²⁷A.M. Kakurin and I.I. Orlovsky, *Plasma Physics Reports* 30, 370 (2004).
- ²⁸R. Jha, D. Raju, and A. Sen, *Physics of Plasmas* 13, 082507 (2006).
- ²⁹E.D. Taylor, C. Cates, M.E. Mauel, D.A. Maurer, D. Nadle, G.A. Navratil, and M. Shilov, *Review of Scientific Instruments* 70, 4545 (1999).
- ³⁰J. Kurzyna, S. Mazouffre, A. Lazurenko, L. Albarde, G. Bonhomme, K. Makowski, M. Dudeck, and Z. Peradzyski, *Physics of Plasmas* 12, 123506 (2005).
- ³¹J. Vaudolon and S. Mazouffre, *Plasma Sources Science and Technology* 24, 032003 (2015).
- ³²R.N. Bracewell, *The Fourier Transform and Its Applications* (McGraw-Hill, New York, 1988).
- ³³M. Mcdonald, C. Bellant, B.S. Pierre, and A. Gallimore, 47th AIAA/ASME/SAE/ASEE Joint Propulsion Conference Amp; Exhibit (2011).